

Deep speckle correlation: a deep learning approach towards scalable imaging through scattering media

Yunzhe Li¹, Yujia Xue¹, Lei Tian^{1,*}

1. *Department of Electrical and Computer Engineering, Boston University, Boston, MA 02215, USA*

* *leitian@bu.edu*

June 22, 2021

Abstract

Imaging through scattering is an important, yet challenging problem. Tremendous progress has been made by exploiting the deterministic input-output relation for a static medium. However, this approach is highly susceptible to speckle decorrelations – small perturbations to the scattering medium lead to model errors and severe degradation of the imaging performance. In addition, this is complicated by the large number of phase-sensitive measurements required for characterizing the input-output ‘transmission matrix’. Our goal here is to develop a new framework that is highly scalable to both medium perturbations and measurement requirement. To do so, we abandon the traditional deterministic approach, instead propose a statistical framework that permits higher representation power to encapsulate a wide range of statistical variations needed for model generalization. Specifically, we develop a convolutional neural network (CNN) that takes intensity-only speckle patterns as input and predicts unscattered object as output. Importantly, instead of characterizing a single input-output relation of a fixed medium, we train our CNN to learn statistical information contained in several scattering media of the same class. We then show that the CNN is able to generalize over a completely different set of scattering media from the same class, demonstrating its superior adaptability to medium perturbations. In our proof of concept experiment, we first train our CNN using speckle patterns captured on diffusers having the same macroscopic parameter (e.g. grits); the trained CNN is then able to make high-quality reconstruction from speckle patterns that were captured from an entirely different set of diffusers of the same grits. To investigate the physical underpinnings of our CNN, we conduct correlation analysis and show that the captured speckle patterns, although are decorrelated (e.g. $< e^{-1}$) using the classical Pearson correlation coefficient metric, still contain statistically invariant information. These invariance is hard to invert using deterministic models, but can be effectively utilized using our statistical CNN model. Our work paves the way to a highly scalable deep learning approach for imaging through scattering media.

1 Introduction

Light scattering in complex media is a pervasive problem across many areas, such as deep tissue imaging [39], and imaging in degraded environment [45]. To date, there is no simple solution for inverting multiple scattering because of the many possible optical paths between the object and the detector. The output of a coherent light scattered from a complex medium exhibits a seemingly random speckle pattern [13]. The speckle’s spatial distribution is a complex function of both the specific arrangement of the scatterers and the wavefront of the incident field. Thus, a comprehensive *deterministic* characterization of the scattering process is often difficult, requiring large-scale measurements.

Major progress has been made by using the framework of transmission matrix (TM) [21, 24, 40, 55], which fully characterizes the input-output relationship of a scattering medium as a linear shift-*variant* matrix. Due to the many underlying degrees of freedom, the size of the TM is inevitably huge, e.g. to transfer a 100×100 pixel image requires a $10^4 \times 10^4$ matrix. In general, the size of the TM grows quadratically as the transferred pixel number, i.e. the space-bandwidth-product (SBP) of the underlying system, making it highly measurement and data-demanding for large-scale, high-SBP applications. Under special circumstances, simplification can be made by utilizing the memory effect [10–12], which essentially approximates the system as linear shift-*invariant*. In practice, however, the SBP from this model is still small due to the limited memory effect range [11, 20, 48], finite sensor’s dynamic range [22], the imaging geometry [30, 36, 54], and trade-off between illumination coherence, speckle contrast, and measurement requirement [4, 9, 22, 28].

A major limitation of the existing *deterministic* approach is its high susceptibility to model errors. The phase-sensitive TM is inherently intolerant to the speckle decorrelation [6, 14, 18, 32, 41, 53, 59]. Slight changes in the arrangement of the scatterers within the medium can lead to much reduced correlations between the speckles measured before and after, which indicates the breakdown of the previous input-output relationship, and thus results in rapid degradation of the transferred images. In other words, a completely new TM needs to be recalibrated once the speckle patterns become decorrelated (e.g. Pearson correlation coefficient $< 1/e$), making this technique challenging to scale for applications involving dynamic scatterers. Current solutions focus on developing hardware with high speed as compared to the decorrelation time of the medium [5, 7, 32, 33, 38, 51, 56]; still, they are only applicable to memory effect-limited field-of-views (FOV), which are restricted to a small SBP.

The goal of this work is to develop a highly *scalable* imaging through scattering framework by overcoming the existing limitations in susceptibility to speckle decorrelation and SBP. The main idea is to build a model that possesses two essential *statistical* properties. First, it can sufficiently encompass the statistical *variations* across media with different scatterer microstructures. Second, it is able to distill

the statistically *invariant* information encoded in the speckle patterns (correlated or decorrelated); this allows the model to be generalizable to the large amounts of objects/media having the same statistical characteristics.

The proposed model is built on a deep learning (DL) framework. To satisfy the desired statistical properties, we do *not* train a convolutional neural network (CNN) to learn the TM of *a single* scattering medium. Instead, *we build a CNN to learn a ‘one-for-all’ mapping by training on several scattering media with different microstructures while having the same macroscopic parameters.* For proof-of-concept, we show that our CNN model trained on a few diffusers can sufficiently support the statistical information of all diffusers having the same mean characteristics (e.g. ‘grits’ [2]). Specifically, we show that the CNN is able to ‘invert’ speckles captured from entirely different diffusers to make high-quality object predictions, as outlined in Fig. 1.

DL is proven to be extremely powerful in solving complex imaging problems, providing performance surpassing those using state-of-the-art model-based techniques [34], such as super-resolution [43, 57], deconvolution [58, 61], compressive imaging [27, 60], tomography [19], holography [42, 44], and phase recovery [37, 50]. Instead of building an explicit model, DL takes a data-driven approach that seeks solutions by learning from large-scale dataset. A major benefit is in its flexibility and adaptability in solving complex problems, in which the exact model is hard to formulate and/or prone to model errors. Closely related to the present work are the learning-based techniques for imaging through scattering [15, 16, 31, 35]. Unfortunately, all existing networks are only trained and tested on the *same* scattering medium, so the model may still be susceptible to speckle decorrelation. Indeed, as tested in our experiment, the CNN model trained on a single diffuser does not capture sufficient statistical variations to interpret speckle patterns from other diffusers. Related to our one-for-all strategy, in non-line-of-sight imaging, a CNN is trained to have superior robustness against variations in experimental parameters for object classification [47].

We demonstrate our technique in a setup subject to *shift-variant* scattering, in which a diffuser is placed in between the object’s real and Fourier space [30, 31, 36]. As shown in [30, 36], this imaging geometry provides a small isoplanatic region (\approx speckle size) so that the memory effect-limited SBP is small, as verified in our experiment (Fig. 2). The objects we aim to recover extend well beyond the memory effect range ($\sim 300 \times 300$ speckle size). In addition, our task is further complicated by the use of coherent illumination while taking intensity-only measurements; the mapping between the object and the speckle’s intensity is nonlinear [13]. The training step in our DL approach is conceptually similar to the TM characterization, in which a series of patterns are input to the scattering medium while the output is measured. In TM characterization, interferometric measurements are typically required to capture the complex field information [21, 24, 40, 55]; an additional iterative phase-retrieval procedure is needed when intensity-only measurements are available [8]. Here, the proposed CNN learns to interpret the ‘phaseless’ measurements using its nonlinear,

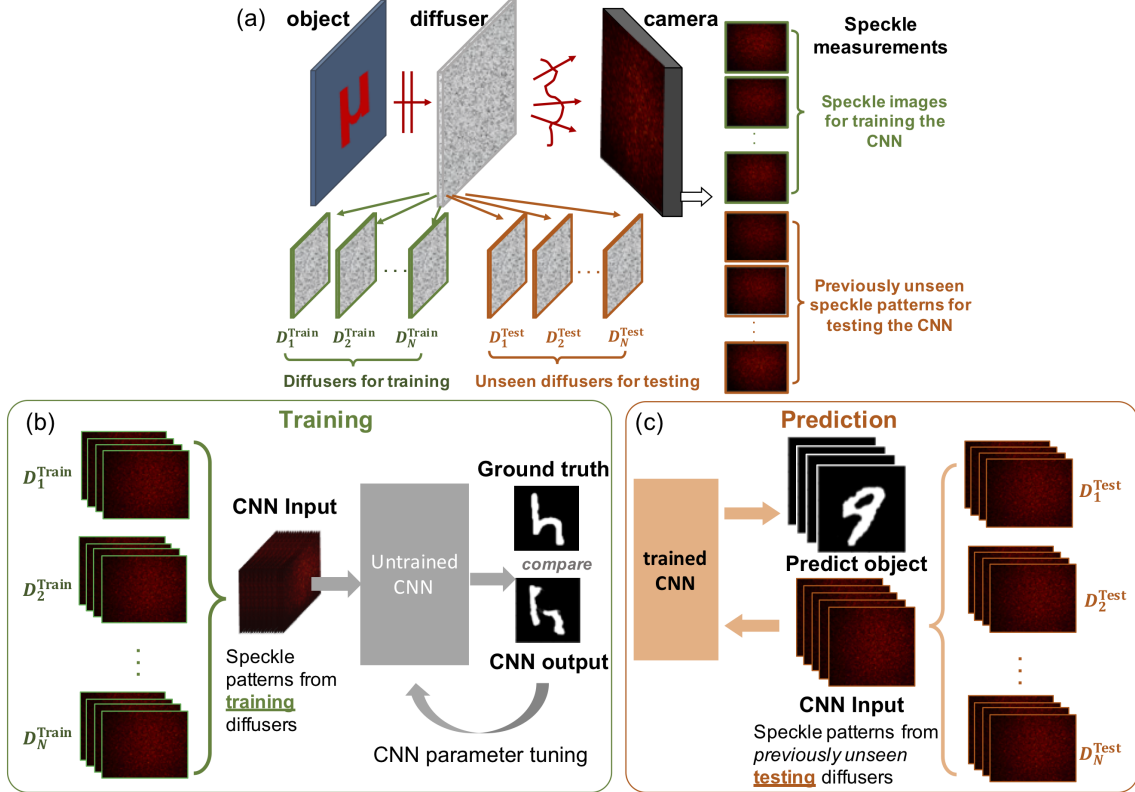


Figure 1: An overview of our deep learning based imaging through scattering technique. (a) Speckle patterns are collected through multiple diffusers. (b) During the training stage, only speckle patterns collected from the *training* diffusers $D_1^{\text{train}}, D_2^{\text{train}}, \dots, D_N^{\text{train}}$ are used. (c) During the testing stage, objects are predicted from speckle patterns collected from *previously unseen testing* diffusers $D_1^{\text{test}}, D_2^{\text{test}}, \dots, D_N^{\text{test}}$, demonstrating the superior scalability of our deep learning approach.

multilayer structure.

We experimentally achieve a $\sim 256 \times 256$ -pixel SBP by using up to 2400 training pairs. To obtain the same SBP, the TM approach would require over 60000 calibration pairs. Importantly, our training data were collected on *multiple* diffusers. Furthermore, distinct from the TM, once our CNN model is trained, it is able to predict objects through diffusers that were *never used during training*. We experimentally quantify the CNN performance trained with 1, 2, or 4 diffusers and demonstrate the superior robustness over speckle decorrelation of our technique.

Although it is hard to derive an explicit expression of our CNN model (a common challenge in all DL techniques [49]), we attempt to provide some physical insights by performing various statistical analysis on our data across multiple objects and diffusers. It is known that the fundamental mechanism of DL is to identify statistical invariance across large datasets [29]. We show that invariance does exist across

seemingly decorrelated speckle patterns taken through different diffusers. Such information would be hard to be directly utilized using existing models. The proposed CNN model is able to automatically discover and exploit these ‘hidden’ invariant features owing to its higher representation power.

Our technique demonstrates a promising DL approach towards a highly scalable framework for imaging through scattering media. It significantly improves the system’s information throughput and adaptability as compared to existing approaches, by improving both the SBP and the robustness to speckle decorrelations.

2 Method

2.1 Experimental setup

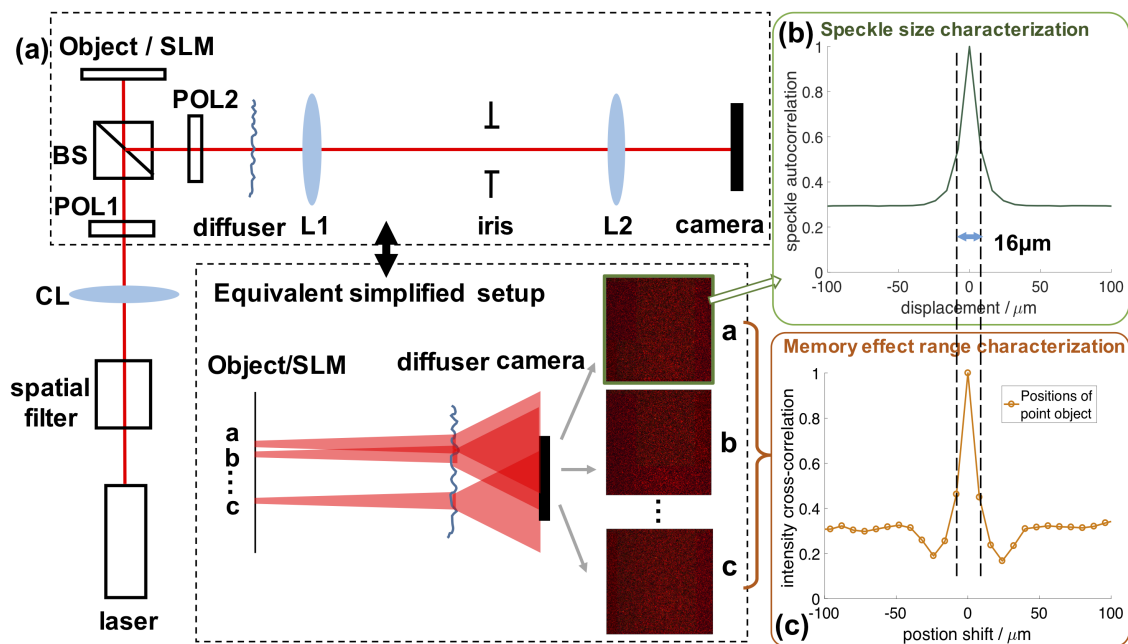


Figure 2: (a) Experimental setup uses an SLM as a programmable object that is illuminated by a laser. A diffuser is placed in between the SLM’s real and Fourier space to create shift-variant scattering. (b) The speckle size is $\sim 16\mu\text{m}$, characterized by the autocorrelation of a speckle pattern. (c) The memory effect range is ~ 1 speckle size characterized by the cross-correlation coefficients between speckle patterns of shifted point objects.

Our experimental setup is shown in Fig. 2(a). A reflective liquid crystal spatial light modulator (SLM) (Holoeye NIR-011, pixel size $8\mu\text{m}$) is used as a programmable *amplitude*-only object by placing two orthogonally oriented polarizers before and after, similar to [31]. To ensure the best modulation contrast, the first polarizer (POL1)

is oriented along the horizontal direction (parallel to the liquid crystal axis) and the second (POL2) is oriented along the vertical direction. The SLM is coherently illuminated by an expanded and collimated beam from a HeNe laser (Thorlabs HNL210L). A 4F system is used to image the SLM onto the camera (Thorlabs Quantalux sCMOS, pixel size $5.04\mu\text{m}$). The 4F system uses two lenses with focal lengths $f_1 = 200\text{mm}$, and $f_2 = 125\text{mm}$ to provide 0.625 magnification. This design approximately produces the same effective pixel size for the object and the image, which is convenient for later CNN training since the same number of pixels can be used for the input and output data without resizing [31]. We note that precise pixel-wise alignment is *not* performed nor needed. An iris is placed at the pupil plane to provide control over the speckle size, which is $\sim 9\text{mm}$ in diameter. The theoretical average speckle size is $\sim 8.8\mu\text{m}$, or equivalently $\sim 14\mu\text{m}$ on the object plane, as set by $\lambda/2\text{NA}$ [13] (NA is the numerical aperture). This is experimentally verified by taking the autocorrelation of a speckle pattern and measuring the full-width at half-maximum [13], which reads $\sim 16\mu\text{m}$, as shown in Fig. 2(b) (for ease of comparison, all length measurements are converted to the object side).

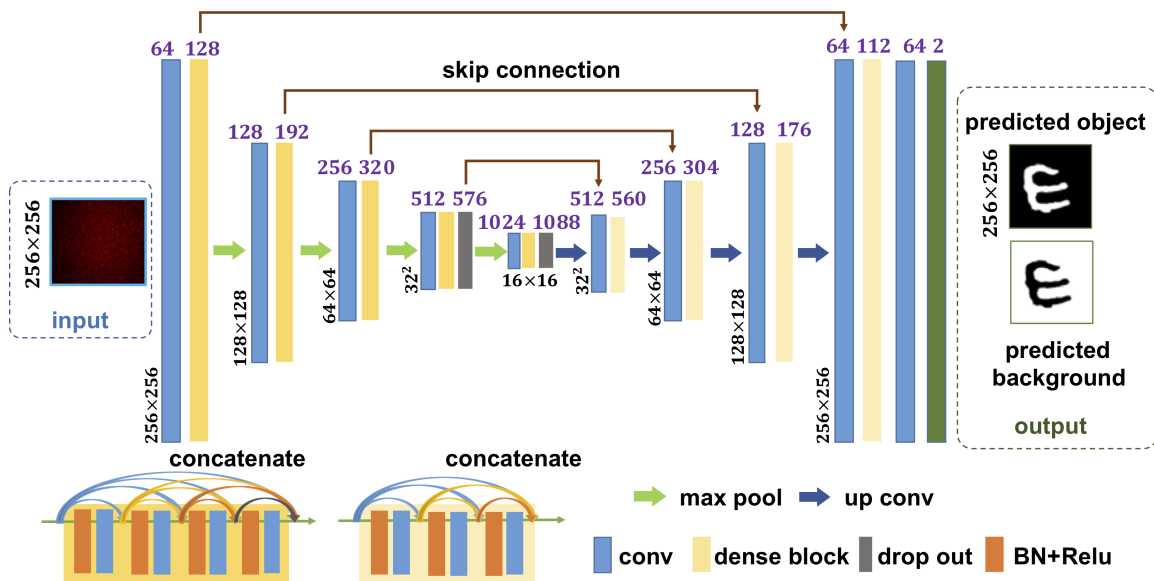


Figure 3: The proposed CNN architecture to learn statistical relationship between speckle patterns and unscattered object. It takes the general encoder-decoder Unet structure. Starting with a high-resolution input speckle pattern, the encoder path gradually condenses the lateral spatial information (size marked in black) into high-level feature maps with growing depths (size marked in purple); the decoder reverses the process by recombining the information into feature maps with gradually increased lateral details; the output consists of a two-channel object, background pixel-wise binary prediction.

The spatially *variant* scattering is generated by placing a ground glass diffuser

(Thorlabs, 220 grits) between the SLM and the first lens (L1) of the 4F system. Under this configuration, the system theoretically only provides a small isoplanatic region whose size is limited to a single speckle size [36]. We quantify the system’s isoplanatic size by performing memory effect range characterization [22]. A 3×3 pixel ‘point-object’ is scanned linearly across the SLM with the minimum step size set by the SLM’s pixel ($8\mu\text{m}$). The memory effect range is then found by calculating the Pearson correlation coefficient between the speckle pattern from the central point and the one from each shifted point. Rapid speckle decorrelation beyond a single speckle range is observed as shown in Fig. 2(c). The correlation coefficient plateaus around 0.3, very close to the value in the speckle intensity autocorrelation curve. The minimum point object size ($24\mu\text{m}$) was limited by the signal-to-background ratios in the experiments due to the imperfect polarizer’s extinction power that generates non-negligible background at low-light levels. The same characterization procedure was repeated on different object sizes; almost identical correlation curves are obtained.

2.2 Data acquisition

The central 512×512 SLM pixels are used as the object; the corresponding central 512×512 camera pixels are used as the raw speckle intensity pattern that are later used for CNN training and testing. Considering the system’s resolution (measured by the speckle size), the SBP is $\sim 300\times 300$ pixels with a field-of-view (FOV) of $\sim 4\times 4$ mm^2 . The object size is well beyond the memory effect range, so the system is highly shift *variant* that requires knowledge about the TM for high-SBP image transfer using existing techniques. The objects displayed on the SLM are 8-bit grayscale images from the MNITS handwritten digit [3] and NIST handwritten letter [1] databases.

In total we take speckle images using 9 different diffusers characterized by the same mean macroscopic parameter, i.e. 220 grits. We use data from up to 4 diffusers to train our CNN, the data from the rest of the 5 diffusers are never seen by the CNN during training and are only used for testing.

To collect the *training* data, we use in-total 600 objects (300 digits and 300 letters). For each *training* diffuser, we take 600 speckle images, giving us in-total up to 2400 training dataset.

Our *testing* data are purposely designed to have three groups for characterizing our CNN’s generalization capability evaluated from different perspectives:

- The first group is to test the generalization over *speckle decorrelation due to the change of micro-structure of diffusers*. It consists of 3000 ‘*seen objects through unseen diffusers*’, which are collected from the *same* 600 objects used in the training, but through the 5 *unseen testing* diffusers.
- The second group tests the generalization capability over *the change of both diffusers and objects*. It consists of 200 ‘*unseen objects through unseen diffusers*’,

collected from previously *unused* 200 objects (100 digits + 100 letters) during the training, and through a randomly selected *unseen testing* diffuser.

- The third group is to benchmark the performance of *the CNN trained on a single diffuser*. It consists of 28 ‘*unseen objects through the same diffuser*’, collected from previously *unused* 28 objects (9 digits + 19 letters) during the training, and through a randomly selected *seen training* diffuser.

2.3 Data preprocessing

Due to the computation and memory limitation, all input and output images are downsampled from 512×512 pixels to 256×256 pixels by taking the average within each 2×2 neighboring pixels. For both training and testing, the input speckle images are normalized between 0 and 1 by dividing each image by its maximum. Although we display grayscale images on the SLM, our CNN is designed to perform a binary detection task that outputs a two-channel binary estimate of the object and background, respectively. Accordingly, during the training, each grayscale object is thresholded by setting all non-zero valued pixels to 1 that gives the ground-truth object; the ground-truth background is the complement.

2.4 CNN implementation

We build a CNN to learn a statistical model relating the speckle patterns and the unscattered objects. Importantly, the goal is to make predictions through previously unseen diffusers.

The proposed CNN structure is sketched in Fig. 3. The overall structure follows the encoder-decoder architecture as ‘Unet’ [46] with modifications made to replace each convolutional layer with a dense block [17] in order to improve the training efficiency, as suggested in [31]. Briefly, the input to the network is a preprocessed 256×256 speckle image. Next, the input image goes through the ‘encoder path’, which consists of 4 dense blocks connected by max pooling layer for downsampling. The intermediate output from the encoder has small lateral dimensions (16×16), but encodes rich information along the ‘depth’ (having 1088 feature maps). Each dense block consists of 4 layers, of which each layer performs batch-normalization (BN), nonlinear activation using the rectified linear unit (ReLU), and convolution (conv) with 4 filters. Next, the low-resolution feature maps go through the ‘decoder path’, which consists of 4 additional dense blocks connected by transposed convolutional layer (up conv) for upsampling. The information across different resolution-scales are tunneled through the encoder-decoder paths by skip connections to preserve high-frequency information. After the decoder path, an additional convolutional layer followed by the last layer produces the final network output. *We emphasize that*

the design of this last layer requires careful consideration and is determined by the specific imaging task. Here, we use the softmax layer to produce a pair of mutually complementary object and background channels.

Our design of the last layer is set by our goal to solve a pixel-wise binary detection problem. First, the CNN makes decisions on if an object is present or not. In addition, it generalizes to objects with arbitrary shape by making such binary decisions pixel-by-pixel. To do so, we use the pixel-averaged binary cross-entropy [46] as the loss function L , given by

$$L = \frac{1}{2N} \sum_c \sum_x -(g \log(p) + (1 - g) \log(1 - p)) \quad (1)$$

where g represents the ground-truth pixel value and p represents the predicted pixel value; the summation is taken over all N -pixels x across both channels c .

Intuitively, the success of the pixel-wise binary detection task relies on the sparsity of the object, which is common in many practical problems. Widely used loss functions, such as mean square error (MSE) and mean absolute error (MAE), cannot promote sparsity since they implicitly assume the underlying object signal to follow Gaussian and Laplace statistics [23]. In contrast, the cross-entropy function naturally promotes sparsity especially in binary problems [52].

The CNN training was performed on the Boston University Shared Computing Cluster with one NVIDIA Tesla P100 GPU using the Keras/Tensorflow framework. Each CNN is trained with 500 epochs using the ADAM optimizer [25] for up to 44 hours. We use a learning rate of 10^{-4} for the first 300 epochs, then 10^{-5} for the next 100 epochs, followed by 10^{-6} for the final 100 epochs. Once the CNN is trained, each prediction was made in real time.

3 Results

We present our results from three types of experiments, in line with the acquired data described in Sec. 22.2. The results from the first two experiments are both from the CNN trained with 4 training diffusers and tested on 5 testing diffusers. The last experiment is to compare the first two results against those from the CNN trained on a single diffuser.

In the first experiment, we test our CNN to *predict ‘seen objects through unseen diffusers’* (a.k.a. Task 1). Notably, our CNN demonstrates superior generalization capability in predicting objects through previously unseen diffusers. Representative examples of the speckle and prediction pairs are shown in Fig. 4. For the same object, although the speckle patterns through different diffusers appear notably different, the CNN can consistently make high-quality predictions. Later, we quantify the differences between these speckle patterns by performing speckle decorrelation analysis

in Sec. 4. The prediction results do present slight variations, because our CNN is functionally making *pixel-wise predictions*, rather than the whole-image classification [26, 47]. Our pixel-wise prediction task is considerably more difficult since the network needs to effectively learn the per-pixel input-output relationship. In addition, since our network adapts to *all diffusers of the same class*, the learned relationship should also be adaptable to all possible statistical variations. The variations of the prediction results is quantified later in Fig. 7.

In the second experiment, we further test our CNN for a more difficult task of *predicting “unseen objects through unseen diffusers”* (a.k.a. Task 2). A quantitative comparison between Task 1 and Task 2 measured by the speckle decorrelation is presented in Sec. 4. Representative examples are shown in Fig. 5, demonstrating that the CNN is able to make high-quality predictions of *unseen objects from the same class as the training objects*, while through unseen diffusers.

In the third experiment, we compare our previous results against those obtained from *the CNN trained on a single diffuser*. The results are presented in Fig. 6, which consists of two sub-tasks. Task 3 makes predictions on *unseen objects by the CNN trained and tested on the same diffuser*. Successful demonstrations of accomplishing this task via machine learning have been reported [15, 16, 31, 35]. Task 4 makes predictions on *unseen objects through a different unseen diffuser by the CNN trained on a single diffuser*. The goals of this experiment are in two folds. First, due to the different choices of network architectures and loss functions, here we validate that our design can indeed reliably perform Task 3, as shown in Fig. 6. Our results are further quantified in Fig. 7, which match the state-of-the-art performance with an average Pearson correlation coefficient score of 0.626 [31]. Second, we verify that a CNN trained on only a single diffuser *cannot* be reliably generalized to other diffusers (shown in Fig. 6), since the CNN is tuned to only fit to the model of a specific diffuser.

Finally, we quantify our performance, and expand our comparisons across 6 CNNs trained on 1, 2, or 4 diffusers with 3 different numbers of training dataset (800, 1600, and 2400). We choose two metrics to evaluate the networks’ performance, including the Jaccard index and Pearson correlation coefficient. The Jaccard index is widely used to measure similarities of binary image pairs [62]. We also report Pearson correlation coefficients for ease of comparison against the state-of-the-art results [31]. Each CNN is tested under the same condition, using the same 1000 speckle patterns covering different objects through 5 testing diffusers. In the top figure of Fig. 7, the Jaccard index of each CNN tested on each individual testing diffuser is shown as a circle. It is seen that results from all 5 unseen diffusers are clustered together, regardless of the CNN is used, demonstrating *the consistency of the CNN prediction against object and diffuser variations*.

The main observations are summarized as follows. First, *the performance improves as more training diffusers are used*. This is evident by comparing the results from the same number of 800 training dataset while increasing the number of training diffusers

(similarly for the 1600 case). Second, *the performance further improves by increasing the number of training dataset*. This is seen by comparing the results from the same number of 4 training diffusers while increases the size of training dataset (similarly for the 2-diffuser case). To provide an intuitive visualization of the metric, the bottom figure of Fig. 7 shows a few representative examples. In the first example, the result is further broken down to visualize the truth positive (in white), the false-positive (in green), and the false-negative (in pink).

The mean Pearson correlation coefficient of each CNN is given in Table 1. It is seen that performance from 4 diffusers and 800 dataset is better than that from 2 diffusers and 1600 dataset (i.e. more diffusers, yet less dataset), further demonstrating the importance of training on multiple diffusers.

Table 1: Pearson correlation coefficient of CNN predictions.

	1 diffuser	2 diffusers	4 diffusers
800 dataset	0.429	0.473	0.568
1600 dataset		0.528	0.577
2400 dataset			0.626

4 Analysis

Although it is hard to provide an analytical expression of our CNN model, still we would like to look for some physical insights of how our CNN works by performing various of correlation analysis on the speckle patterns. It has been shown that the main principle of DL to learn statistical invariant information across large data [29]. Thus, our goal is to look for *any physically meaningful invariant patterns/features* for speckles taken through different diffusers. If found any, it can suggest that it is physically plausible to establish a statistical mapping to relate these speckles by our CNN model. A summary of our findings is presented in Fig. 8.

First, we quantify speckle decorrelation in our measurement using the classical Pearson correlation coefficient metric [6, 14, 18, 32, 41, 53, 59]. Figure 8(a) presents the coefficients' histograms under three Tasks (defined in Sec. 3), each from 400 randomly chosen speckle patterns. We describe the result based on the order of decorrelation (hence the difficulty of the task). First, Task 3 (Fig. 6) is evaluated by $A_{D1} * B_{D1}$, which correlates speckles from *different objects through the same diffuser*. Most of the speckle patterns are decorrelated and the mean coefficient is 0.307, which is consistent with the values found in both memory effect and speckle size characterization plots in Fig. 2(c). Second, Task 1 (Fig. 4) is evaluated by $A_{D1} * A_{D2}$, which is for *the same object through different diffusers*. The speckle patterns are further decorrelated to a mean value of 0.221. Third, Task 2 (Fig. 5) is evaluated by $A_{D1} * B_{D2}$, which is

for *different objects through different diffusers*. This gives the lowest correlation of around 0.207.

A single-valued metric does not sufficiently capture the rich information encoded in the speckle patterns. As inspired by speckle correlography [28] and its variants [4, 9, 22], next we investigate the speckle intensity correlation function for different speckle pattern pairs. Representative examples from our main findings are presented in Fig. 8(b). *Importantly, taking the speckle intensity autocorrelation as the reference, speckle intensity cross-correlation from the same object but through two different diffusers (i.e. the first for training, and the second for testing) resembles the similar pattern as the reference.* These correlation patterns do not follow the simple relation exploited in [4, 9, 22, 28]. Nevertheless, the *invariance* maintained across speckle patterns *from training and testing diffusers* do suggest that there exist *learnable* and *generalizable* features. Our CNN model is able to discover and exploit these ‘hidden’ information albeit these speckle pairs are considered “decorrelated” based on the Pearson correlation coefficient metric. Next, correlation patterns from visually similar objects are shown to present notable difference, which demonstrates the sensitivity of these features. Overall, we speculate that these invariant correlation patterns/features could contribute to the scalability of our CNN with respect to speckle decorrelations.

5 Conclusion

We have demonstrated a deep learning framework to significantly improve the scalability of imaging through scattering. Traditional techniques suffer from the ‘*one-for-one*’ limitation, in which one model only works for one fixed scattering medium. Here, we take an entirely different ‘*one-for-all*’ strategy, in which one model can fit to all scattering media within the same class. In practice, this leads to significantly improved resilience to speckle decorrelations and improved space-bandwidth-product. Upon further development, this deep learning approach promises highly scalable, large information-throughput imaging through complex scattering media.

Code availability

Code in this manuscript is available upon request to the corresponding author.

Acknowledgments

We thank Xiaojun Cheng for helpful discussions on correlation analysis. Funding was provided by National Science Foundation (NSF) (1711156).

Conflict of interest

The authors declare no conflict of interest.

References

- [1] <https://www.nist.gov/srd/nist-special-database-19>.
- [2] <https://www.unc.edu/~rowlett/units/scales/grit.html>.
- [3] <http://yann.lecun.com/exdb/mnist/>.
- [4] J. Bertolotti, E. G. van Putten, C. Blum, A. Lagendijk, W. L. Vos, and A. P. Mosk. Non-invasive imaging through opaque scattering layers. *Nature*, 491(7423):232–234, 2012.
- [5] B. Blochet, L. Bourdieu, and S. Gigan. Focusing light through dynamical samples using fast continuous wavefront optimization. *Optics Letters*, 42(23):4994–4997, 2017.
- [6] J. Brake, M. Jang, and C. Yang. Analyzing the relationship between decorrelation time and tissue thickness in acute rat brain slices using multispeckle diffusing wave spectroscopy. *JOSA A*, 33(2):270–275, 2016.
- [7] D. Conkey, A. Caravaca-Aguirre, and R. Piestun. High-speed scattering medium characterization with application to focusing light through turbid media. *Optics Express*, 20(2):1733–1740, 2012.
- [8] A. Drémeau, A. Liutkus, D. Martina, O. Katz, C. Schülke, F. Krzakala, S. Gigan, and L. Daudet. Reference-less measurement of the transmission matrix of a highly scattering material using a dmd and phase retrieval techniques. *Optics Express*, 23(9):11898–11911, 2015.
- [9] E. Edrei and G. Scarcelli. Optical imaging through dynamic turbid media using the Fourier-domain shower-curtain effect. *Optica*, 3(1):71–74, 2016.
- [10] S. Feng, C. Kane, P. A. Lee, and A. D. Stone. Correlations and fluctuations of coherent wave transmission through disordered media. *Physical Review Letters*, 61(7):834, 1988.
- [11] I. Freund. Looking through walls and around corners. *Physica A: Statistical Mechanics and its Applications*, 168(1):49–65, 1990.
- [12] I. Freund, M. Rosenbluh, and S. Feng. Memory effects in propagation of optical waves through disordered media. *Physical Review Letters*, 61(20):2328, 1988.

- [13] J. W. Goodman. *Speckle phenomena in optics: theory and applications*. Roberts and Company Publishers, 2007.
- [14] T. R. Hillman, T. Yamauchi, W. Choi, R. R. Dasari, M. S. Feld, Y. Park, and Z. Yaqoob. Digital optical phase conjugation for delivering two-dimensional images through turbid media. *Scientific Reports*, 3:1909, 2013.
- [15] R. Horisaki, R. Takagi, and J. Tanida. Learning-based imaging through scattering media. *Optics Express*, 24(13):13738–13743, 2016.
- [16] R. Horisaki, R. Takagi, and J. Tanida. Learning-based focusing through scattering media. *Applied Optics*, 56(15):4358–4362, 2017.
- [17] G. Huang, Z. Liu, L. v. d. Maaten, and K. Q. Weinberger. Densely connected convolutional networks. In *2017 IEEE Conference on Computer Vision and Pattern Recognition (CVPR)*, pages 2261–2269, July 2017.
- [18] M. Jang, H. Ruan, I. M. Vellekoop, B. Judkewitz, E. Chung, and C. Yang. Relation between speckle decorrelation and optical phase conjugation (OPC)-based turbidity suppression through dynamic scattering media: a study on in vivo mouse skin. *Biomedical Optics Express*, 6(1):72–85, 2015.
- [19] K. H. Jin, M. T. McCann, E. Froustey, and M. Unser. Deep convolutional neural network for inverse problems in imaging. *IEEE Transactions on Image Processing*, 26(9):4509–4522, 2017.
- [20] B. Judkewitz, R. Horstmeyer, I. M. Vellekoop, I. N. Papadopoulos, and C. Yang. Translation correlations in anisotropically scattering media. *Nature Physics*, 11(8):684, 2015.
- [21] S. Kang, S. Jeong, W. Choi, H. Ko, T. D. Yang, J. H. Joo, J.-S. Lee, Y.-S. Lim, Q.-H. Park, and W. Choi. Imaging deep within a scattering medium using collective accumulation of single-scattered waves. *Nature Photonics*, 9(4):253–258, 2015.
- [22] O. Katz, P. Heidmann, M. Fink, and S. Gigan. Non-invasive single-shot imaging through scattering layers and around corners via speckle correlations. *Nature Photonics*, 8(10):784–790, 2014.
- [23] A. Kendall and Y. Gal. What uncertainties do we need in bayesian deep learning for computer vision? In *Advances in Neural Information Processing Systems*, pages 5580–5590, 2017.
- [24] M. Kim, W. Choi, Y. Choi, C. Yoon, and W. Choi. Transmission matrix of a scattering medium and its applications in biophotonics. *Optics Express*, 23(10):12648–12668, 2015.

- [25] D. P. Kingma and J. Ba. Adam: A method for stochastic optimization. *CoRR*, abs/1412.6980, 2014.
- [26] A. Krizhevsky, I. Sutskevar, and G. Hinton. Imagenet classification with deep convolutional neural networks. In *Proc. Advances in Neural Information Processing Systems 25*, pages 1097–1105, Lake Tahoe, NV, USA, December 3-8, 2012.
- [27] K. Kulkarni, S. Lohit, P. Turaga, R. Kerviche, and A. Ashok. Reconnet: Non-iterative reconstruction of images from compressively sensed measurements. In *Proceedings of the IEEE Conference on Computer Vision and Pattern Recognition*, pages 449–458, 2016.
- [28] A. Labeyrie. Attainment of diffraction limited resolution in large telescopes by fourier analysing speckle patterns in star images. *Astron. Astrophys*, 6(1):85–87, 1970.
- [29] Y. LeCun, Y. Bengio, and G. Hinton. Deep learning. *Nature*, 521(7553):436–444, 2015.
- [30] J. Li, D. R. Beaulieu, H. Paudel, R. Barankov, T. G. Bifano, and J. Mertz. Conjugate adaptive optics in widefield microscopy with an extended-source wavefront sensor. *Optica*, 2(8):682–688, 2015.
- [31] S. Li, M. Deng, J. Lee, A. Sinha, and G. Barbastathis. Imaging through glass diffusers using densely connected convolutional networks. *arXiv preprint arXiv:1711.06810*, 2017.
- [32] Y. Liu, P. Lai, C. Ma, X. Xu, A. A. Grabar, and L. V. Wang. Optical focusing deep inside dynamic scattering media with near-infrared time-reversed ultrasonically encoded (TRUE) light. *Nature Communications*, 6:5904, 2015.
- [33] Y. Liu, C. Ma, Y. Shen, J. Shi, and L. V. Wang. Focusing light inside dynamic scattering media with millisecond digital optical phase conjugation. *Optica*, 4(2):280–288, 2017.
- [34] A. Lucas, M. Iliadis, R. Molina, and A. K. Katsaggelos. Using deep neural networks for inverse problems in imaging. *IEEE Signal Processing Magazine*, 1053(5888/18), 2018.
- [35] M. Lyu, H. Wang, G. Li, and G. Situ. Exploit imaging through opaque wall via deep learning. *arXiv preprint arXiv:1708.07881*, 2017.
- [36] J. Mertz, H. Paudel, and T. G. Bifano. Field of view advantage of conjugate adaptive optics in microscopy applications. *Applied Optics*, 54(11):3498–3506, 2015.

- [37] T. Nguyen, Y. Xue, Y. Li, L. Tian, and G. Nehmetallah. Convolutional neural network for Fourier ptychography video reconstruction: learning temporal dynamics from spatial ensembles. *arXiv preprint arXiv:1805.00334*, 2018.
- [38] M. Nixon, O. Katz, E. Small, Y. Bromberg, A. A. Friesem, Y. Silberberg, and N. Davidson. Real-time wavefront shaping through scattering media by all-optical feedback. *Nature Photonics*, 7(11):919, 2013.
- [39] V. Ntziachristos. Going deeper than microscopy: the optical imaging frontier in biology. *Nat. Methods*, 7(8):603–614, August 2010.
- [40] S. Popoff, G. Lerosey, R. Carminati, M. Fink, A. Boccarda, and S. Gigan. Measuring the transmission matrix in optics: an approach to the study and control of light propagation in disordered media. *Physical Review Letters*, 104(10):100601, 2010.
- [41] M. M. Qureshi, J. Brake, H.-J. Jeon, H. Ruan, Y. Liu, A. M. Safi, T. J. Eom, C. Yang, and E. Chung. In vivo study of optical speckle decorrelation time across depths in the mouse brain. *Biomedical Optics Express*, 8(11):4855–4864, 2017.
- [42] Z. Ren, Z. Xu, and E. Y. Lam. Learning-based nonparametric autofocusing for digital holography. *Optica*, 5(4):337–344, Apr 2018.
- [43] Y. Rivenson, Z. Göröcs, H. Günaydin, Y. Zhang, H. Wang, and A. Ozcan. Deep learning microscopy. *Optica*, 4(11):1437–1443, 2017.
- [44] Y. Rivenson, Y. Zhang, H. Günaydin, D. Teng, and A. Ozcan. Phase recovery and holographic image reconstruction using deep learning in neural networks. *Light: Science & Applications*, 7(2):17141, 2018.
- [45] M. C. Roggemann, B. M. Welsh, and B. R. Hunt. *Imaging through turbulence*. CRC press, 2018.
- [46] O. Ronneberger, P. Fischer, and T. Brox. U-net: Convolutional networks for biomedical image segmentation. In *International Conference on Medical image computing and computer-assisted intervention*, pages 234–241. Springer, 2015.
- [47] G. Satat, M. Tancik, O. Gupta, B. Heshmat, and R. Raskar. Object classification through scattering media with deep learning on time resolved measurement. *Optics Express*, 25(15):17466–17479, 2017.
- [48] S. Schott, J. Bertolotti, J.-F. Léger, L. Bourdieu, and S. Gigan. Characterization of the angular memory effect of scattered light in biological tissues. *Optics Express*, 23(10):13505–13516, 2015.

- [49] R. Shwartz-Ziv and N. Tishby. Opening the black box of deep neural networks via information. *arXiv preprint arXiv:1703.00810*, 2017.
- [50] A. Sinha, J. Lee, S. Li, and G. Barbastathis. Lensless computational imaging through deep learning. *Optica*, 4(9):1117–1125, 2017.
- [51] C. Stockbridge, Y. Lu, J. Moore, S. Hoffman, R. Paxman, K. Toussaint, and T. Bifano. Focusing through dynamic scattering media. *Optics Express*, 20(14):15086–15092, 2012.
- [52] S. Suresh, N. Sundararajan, and P. Saratchandran. Risk-sensitive loss functions for sparse multi-category classification problems. *Information Sciences*, 178(12):2621–2638, 2008.
- [53] X. Tao, D. Bodington, M. Reinig, and J. Kubby. High-speed scanning interferometric focusing by fast measurement of binary transmission matrix for channel demixing. *Optics Express*, 23(11):14168–14187, 2015.
- [54] A. Tokovinin, M. Le Louarn, and M. Sarazin. Isoplanatism in a multiconjugate adaptive optics system. *JOSA A*, 17(10):1819–1827, 2000.
- [55] E. G. van Putten and A. P. Mosk. Viewpoint: The information age in optics: Measuring the transmission matrix. *Physics*, 3:22, 2010.
- [56] D. Wang, E. H. Zhou, J. Brake, H. Ruan, M. Jang, and C. Yang. Focusing through dynamic tissue with millisecond digital optical phase conjugation. *Optica*, 2(8):728–735, 2015.
- [57] H. Wang, Y. Rivenson, Y. Jin, Z. Wei, R. Gao, H. Gunaydin, L. Bentolila, and A. Ozcan. Deep learning achieves super-resolution in fluorescence microscopy. *bioRxiv*, page 309641, 2018.
- [58] L. Xu, J. S. Ren, C. Liu, and J. Jia. Deep convolutional neural network for image deconvolution. In *Advances in Neural Information Processing Systems*, pages 1790–1798, 2014.
- [59] X. Yang, Y. Pu, and D. Psaltis. Imaging blood cells through scattering biological tissue using speckle scanning microscopy. *Optics Express*, 22(3):3405–3413, 2014.
- [60] H. Yao, F. Dai, D. Zhang, Y. Ma, S. Zhang, and Y. Zhang. Dr2-net: Deep residual reconstruction network for image compressive sensing. *arXiv preprint arXiv:1702.05743*, 2017.
- [61] M. D. Zeiler, D. Krishnan, G. W. Taylor, and R. Fergus. Deconvolutional networks. In *Computer Vision and Pattern Recognition (CVPR), 2010 IEEE Conference on*, pages 2528–2535. IEEE, 2010.

- [62] K. H. Zou, S. K. Warfield, A. Bharatha, C. M. Tempany, M. R. Kaus, S. J. Haker, W. M. Wells, F. A. Jolesz, and R. Kikinis. Statistical validation of image segmentation quality based on a spatial overlap index1: scientific reports. *Academic Radiology*, 11(2):178–189, 2004.

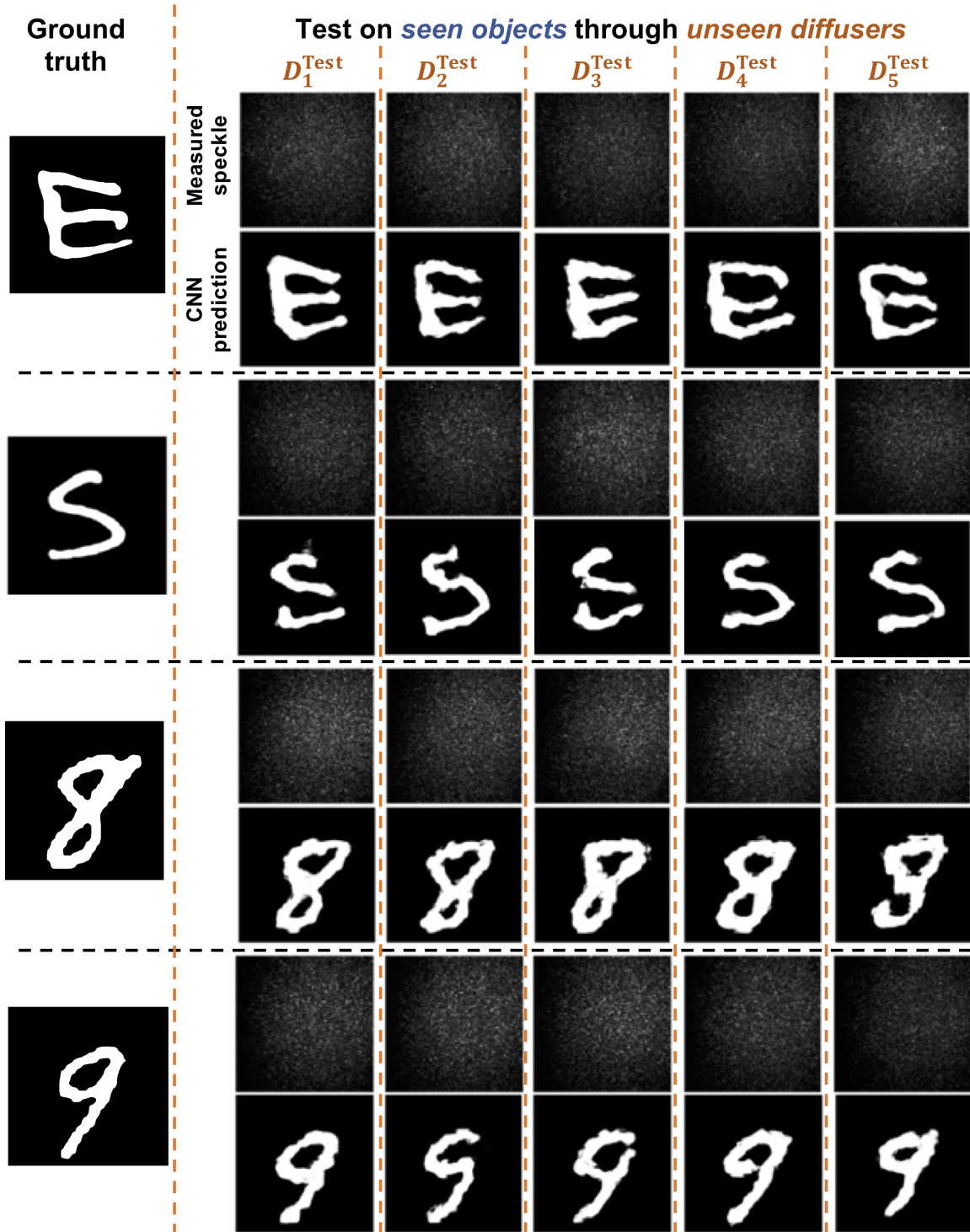


Figure 4: Testing results of ‘seen objects through unseen diffusers’. The *single* CNN trained with four ‘training diffusers’ is used to predict objects through previously unseen ‘testing diffusers’, $D_1^{\text{test}}, D_2^{\text{test}}, D_3^{\text{test}}, D_4^{\text{test}}, D_5^{\text{test}}$. The same set of objects are used during the training through the training diffusers. Despite the apparent differences across the speckle patterns, consistently reliable predictions are made by our CNN.

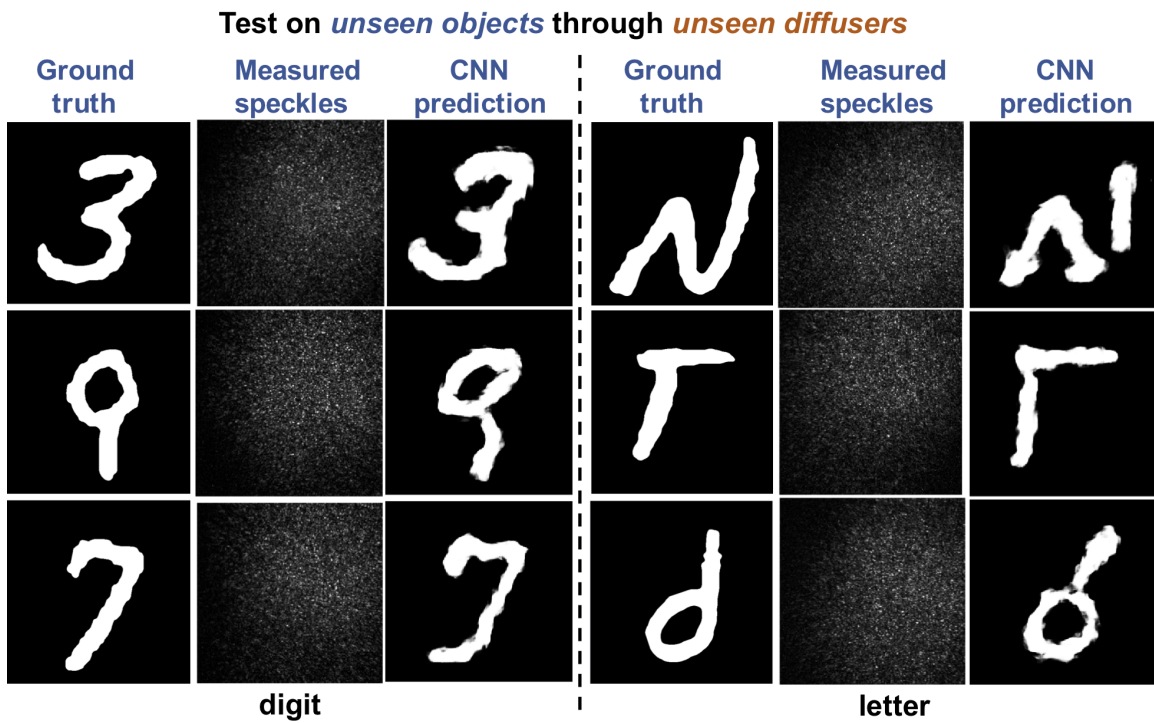


Figure 5: Testing results of ‘unseen objects through unseen diffusers’. The CNN trained with four ‘training diffusers’ is tested to make predictions based on speckles from previously unused objects (during training) through previously unseen testing diffusers.

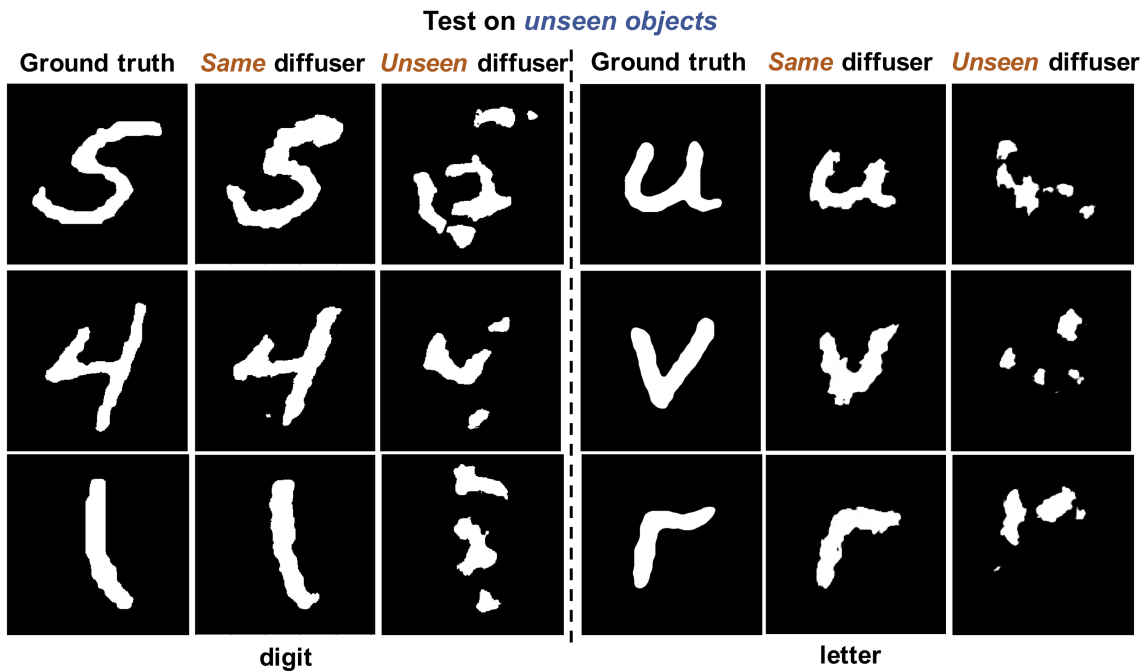


Figure 6: Testing results of the CNN trained on *a single diffuser*. When tested with speckles from unseen object (during training) through the *same* diffuser, the CNN is able to make high-quality prediction. However, the CNN fails when tested on speckles from a different unseen diffuser, demonstrating the importance of our proposed learning strategy involving multiple diffusers.

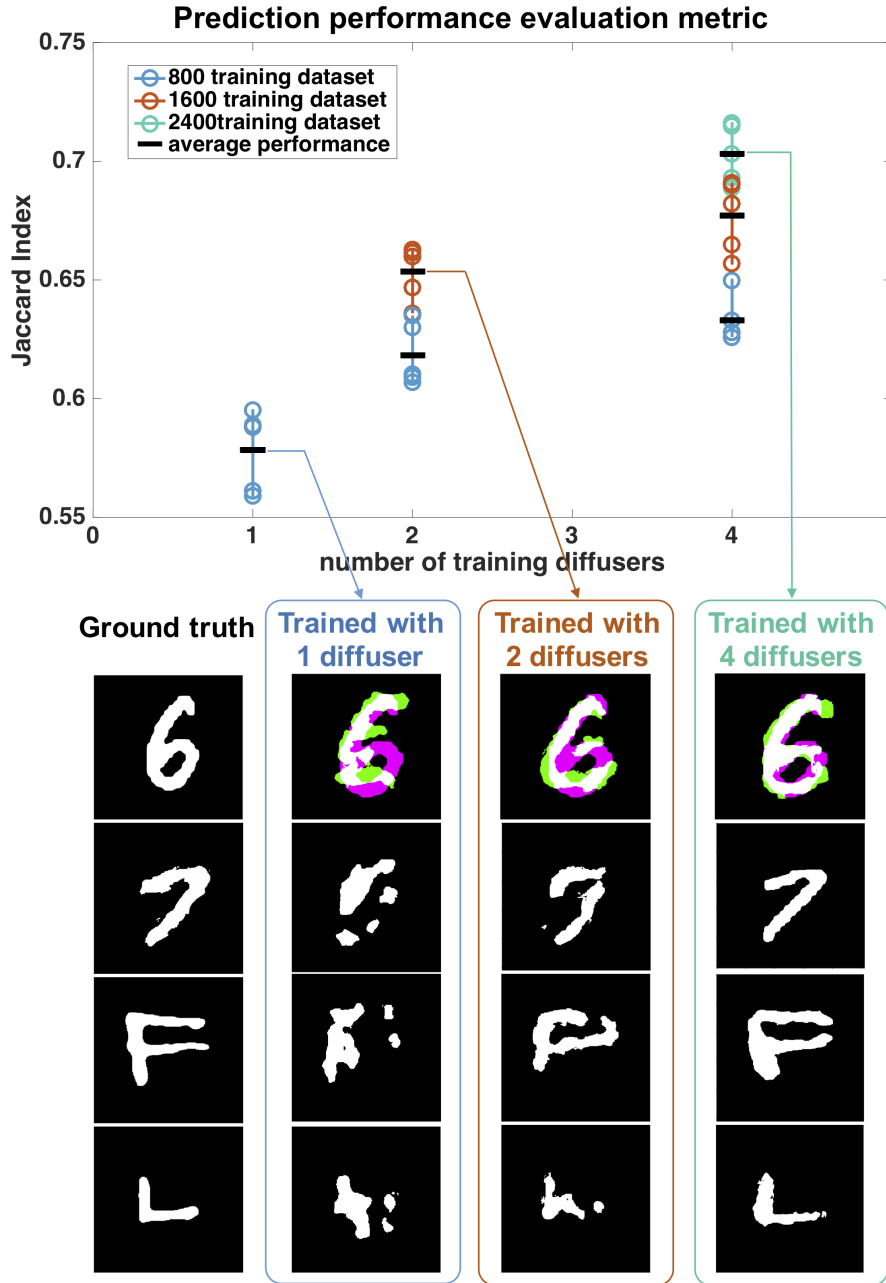


Figure 7: We compare the performance of multiple CNNs trained on 1, 2, and 4 diffusers using different numbers of dataset (800 in blue, 1600 in orange, 2400 in green) using the Jaccard index metric. Each CNN is tested under the same condition, using the same 1000 speckle patterns covering different objects through 5 testing diffusers. Each circle represents the average performance on all objects through an individual testing diffuser. The mean performance of each CNN is marked by black horizontal bars. The bottom figure shows representative example predictions from the CNN trained on 1, 2, and 4 diffusers, respectively. To better visualize the result, the first example shows the CNN prediction that is overlaid with the true-positive (in white), the false-positive (in green), and the false-negative (in pink).

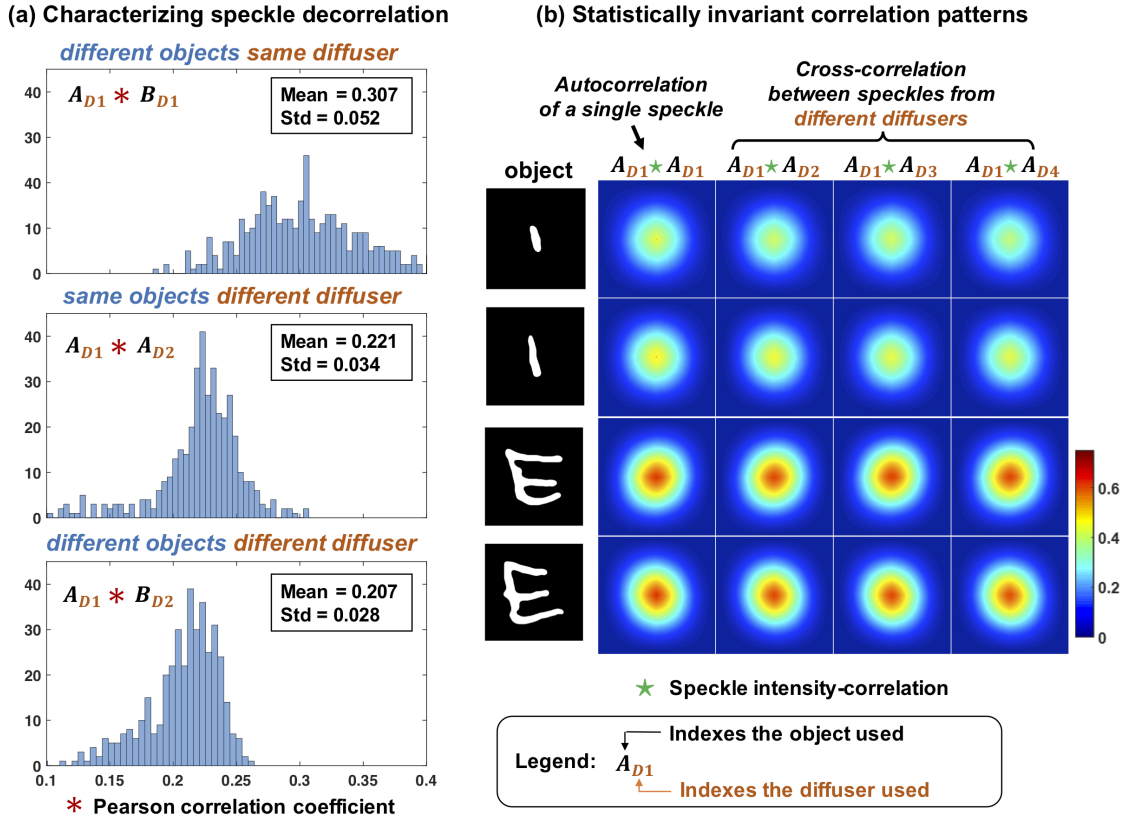


Figure 8: (a) To quantitatively analyze the robustness of our CNN to speckle decorrelations, Pearson correlation coefficients are calculated based on randomly selected 400 speckle patterns for three different cases: $A_{D1} * B_{D1}$: different objects, the same diffuser; $A_{D1} * A_{D2}$: the same object, different diffusers; $A_{D1} * B_{D2}$: different objects, different diffusers. The results show progressively more difficult tasks tested in our experiments. Training and testing on the same diffuser (Fig. 6) needs to overcome an average 0.307 decorrelation; training on one diffuser and testing on another diffuser but with the same object (Fig. 4) needs to account for an average 0.221 decorrelation; training and testing on different objects and diffusers (Fig. 5) needs to further model an average 0.207 decorrelation. (b) Correlating speckle patterns from the same objects but through different diffusers shows invariant patterns, which provides a possible source of weak correlation information exploited by the CNN.